# Hierarchical Hybrid Organic–Inorganic Materials with Tunable Textural Properties Obtained Using Zeolitic-Layered Precursor

Maksym Opanasenko,[†,‡] Wallace O'Neil Parker, Jr.,[§] Mariya Shamzhy,[†,‡] Erica Montanari,[§] Michela Bellettato,[§] Michal Mazur,[†] Roberto Millini,[§] and Jiří Čejka*,[†]

[†]J. Heyrovský Institute of Physical Chemistry, Academy of Sciences of Czech Republic, v.v.i. Dolejškova 3, 182 23 Prague 8, Czech Republic

[‡]L.V. Pisarzhevskiy Institute of Physical Chemistry, National Academy of Sciences of Ukraine, 31 pr. Nauky, Kyiv 03028, Ukraine

[§]Eni S.p.A., Refining & Marketing Division, San Donato Milanese Research Center, Physical Chemistry Dept., via F. Maritano 26, I-20097 San Donato Milanese, Italy

Ⓢ *Supporting Information*

**ABSTRACT:** Novel layered zeolitic organic–inorganic materials have been synthesized using a two-dimensional zeolite precursor IPC-1P prepared by a top-down approach from zeolite **UTL**. The formation of porous materials containing organic linkers or polyhedral oligomeric siloxane covalently bonded to zeolite layers in the interlayer space was confirmed by a variety of characterization techniques ($N_2$/Ar sorption analysis, XRD, $^{29}$Si and $^{13}$C NMR, TEM). The organic–inorganic porous hybrids obtained by intercalation with silsesquioxane posessed layered morphology and contained large crystalline domains. The hybrids exhibited mesoporous or hierarchical micro-/mesoporous systems, stable up to 350 °C. Textural properties of the formed zeolitic organic–inorganic materials can be controlled by varying the linker or synthetic conditions over a broad range. Surface areas and pore volumes of synthesized hybrids significantly exceed those for parent zeolite **UTL** and corresponding swollen material; the amount of micropores increased with increasing rigidity and size of the organic linker in the order biphenyl > phenylene > ethanediyl.
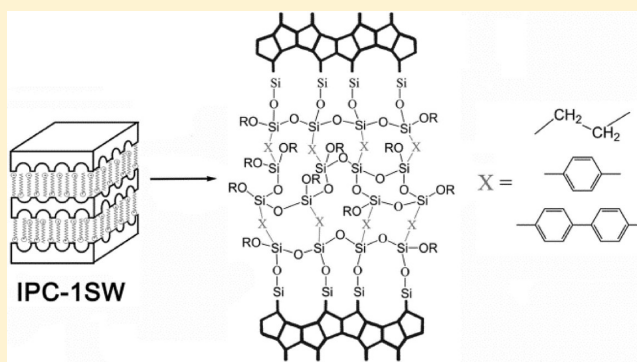
## ■ INTRODUCTION

The multifunctional structured porous hybrid materials (covalently bonded organic–inorganic nanosystems) are of considerable interest for applications in separation, catalysis and optics.[1–6] Such materials can combine the advantages of inorganic (thermal, mechanical and structural stability) and organic parts (possibility for functionalization and high flexibility).[7,8]

Different synthesis protocols for functionalization of microporous materials have been proposed. Postsynthesis treatment of preformed aluminosilicates with organosilanes was investigated using series of **FAU** zeolites containing mesopores.[9–12] It was found that the functionalization practically does not occur within the micropores but only in the mesopores and on the external surface. More interesting was the co-condensation approach proposed by Jones et al., providing organic functionalized molecular sieves (OFMSs) by replacing a part of the conventional silica source (e.g., TEOS) with an organosilane (e.g., phenethyltrimethoxysilane, aminopropyltrimethoxysilane, mercaptopropyltrimethoxysilane) in the reaction mixture.[13–16] Although successful, this protocol suffers from a severe drawback: it can be applied only for

functionalizing zeolites, from which the organic structure directing agent (SDA) needs be removed by chemical extraction and not by high-temperature thermal treatments. As a matter of fact, all the work was done using zeolite **Beta**, from which the tetraethylammonium was removed by repeated treatments with acetic acid/water solutions.

Another method consists of the replacement of the framework oxygen atoms by incorporation of bivalent organic groups in the framework. Using this approach, hybrid organic–inorganic materials with the **MFI**, **LTA**, **Beta**, or **FAU** framework structure were synthesized with bis-(triethoxysilyl)-methane and bis-(triethoxysilyl)ethane.[17–21] In all cases, the content of carbon in the final product was much lower than the theoretical one, corresponding to the replacement of 25% maximum of the framework oxygen atoms. In addition, the crystallization rate of the corresponding hybrid is very low compared to the conventional synthesis and crystallization does not occur under nearly neutral conditions. This means that crystallization only takes place when $[SiO_4]$ tetrahedra are

available in the reaction mixture and they can be produced *via* hydrolysis of the Si−C bond or added as a second conventional silica source (e.g., TEOS). In any case, the possibility of synthesizing hybrid organic−inorganic zeolites was not unambiguously demonstrated since none of the characterization techniques employed so far can distinguish an alkanediyl group incorporated in the zeolite framework from that contained in the amorphous phase which is usually present even in trace amounts in the products.[21]

More recently, porous crystalline organic−inorganic aluminosilicates were synthesized hydrothermally at 100 °C from an aqueous mixture containing a disilane of general formula $(R'O)_3Si-R-Si(OR')_3$ (with R = $-C_6H_4-$, $-C_6H_4-C_6H_4-$, $-(CH_2)_2-C_6H_4-(CH_2)_2-$ or $-(CH_2)_3-$ and R' = $-CH_3$ or $-CH_2CH_3$), $NaAlO_2$, NaOH and/or KOH.[22] The members of this new class of materials, called Eni Carbon Silicates (ECSs), invariably consist of a regular stacking of aluminosilicate layers covalently connected by organic groups.[22−24] The arrangement of the disilane moieties generates regular microporosity: inaccessible cages, formed by six phenylene rings in ECS-2,[22] large and accessible sinusoidal channels running parallel to the inorganic layers in ECS-3,[23] and large cylindrical straight channels perpendicular to the inorganic layers in ECS-14.[24] It is worth noting that the inorganic layers of ECS materials are formed by the assembly of secondary building units usually found in zeolite frameworks and the strict analogy with "zeotype materials" was confirmed by the structure of ECS-14, whose inorganic layers possess the **AFI** framework topology.[24] Accordingly, ECS materials can be considered as the pillaring of zeolite layers with covalently bonded organic groups. Considering the above comments, the use of layered inorganic precursors seems to be one of the most efficient routes to obtain novel materials[25−27] including organic−inorganic hybrids with organic "linkers" between the inorganic layers.[28−30]

Charged layered inorganic precursors (i.e., clays,[31−35] micas,[36] hydrotalcites[37]) with ion-exchange capacity have been used to generate organosilicates by incorporation of organic compounds (tetraalkylammonium, aminoacids, polyalcohols, zwitterionic surfactants, etc.) in the interlayer space. Different layered sodium silicates (magadiite, ilerite, octosilicate) were used to prepare two- or three-dimensional hybrid porous materials by intercalation with alkylsilanes, chlorosilanes or bridged silsesquioxanes.[29,38−42] But the relatively weak stability, structural disorder and poor crystallinity of such materials hinder their potential applications, unlike the materials obtained using layered zeolite precursors.[43] Moderately stable hybrid materials were prepared by Corma's group[30] using zeolitic layers of the **MWW** precursor (MCM-22P) as building units and using bridged silsesquioxanes as pillars. Postsynthesis treatments of these zeolitic hybrids (functionalization of the organic counterpart with basic amino groups) resulted in the formation of bifunctional acid−base catalysts. Catalytic activity for the prepared materials was demonstrated in a one-pot synthesis of benzylidene malononitrile from malononitrile and benzaldehyde dimethylacetal by acetal hydrolysis and Knoevenagel condensation.[30]

Recently, it was shown that **UTL** zeolite is also a promising material for structure postsynthesis modifications including hydrolysis to give two-dimensional (2D) layers, pillaring or even further condensation to new zeolites IPC-2 and **PCR** using the so-called "top-down" approach.[25,26,43]

The aim of this contribution is to present the synthesis and properties of novel, layered, hybrid zeolite-based materials prepared by pillaring IPC-1P (a precursor obtained by top-down synthesis from **UTL** zeolite) with bridged silsesquioxanes (BSS) or using a polyhedral oligomeric siloxane (POS). The synthetic protocol described here provides pillared materials formed from inorganic layers, connected with organic or well-defined inorganic pillars, exhibiting substantially larger surface areas and controlled porosities of the interlamellar space than those published up to now.

## EXPERIMENTAL SECTION

**Synthesis of SDA Template.** Preparation of 7-ethyl-6-azoniaspiro-[5.5]-undecane hydroxide was carried out using a method similar to the process in ref 44. For this purpose, distilled water (70 mL), sodium hydroxide (2.84 g), and 1,4-dibromopentane (16.22 g) were mixed in a round-bottom flask. Then, 2-ethylpiperidine (8.03 g) was added. The mixture was vigorously stirred (12 h) to prepare a suspension and cooled down in an ice bath. A cooled solution of sodium hydroxide (40 mL, 50 wt %) was added to the suspension. After that, solid sodium hydroxide (10 g) was added slowly under vigorous stirring with continuous cooling. The addition of sodium hydroxide was stopped after reaching the saturation of water solution. Further intensive stirring resulted in the formation of the white crystals, which were recovered by filtration and extracted three times with chloroform (100 mL). The organic fractions were dried using anhydrous sodium sulfate and were partially evaporated. The ammonium salt was precipitated and washed with diethyl ether. Product was converted into the hydroxide form by ion exchange with AG 1-X8 (Bio-Rad) resin. The successful synthesis of this structure-directing agent (SDA) was confirmed by ^{1}H NMR spectroscopy (Figure S2, Supporting Information [SI]).

**Synthesis of UTL.** UTL zeolite was synthesized similarly to the process in ref 45. A reaction gel with the molar composition 0.8 $SiO_2$: 0.4 $GeO_2$: 0.5 SDA: 30 $H_2O$ was prepared by dissolution of germanium oxide (Aldrich) in an SDA hydroxide solution. Then silica (Cab-O-Sil M5) was added to the solution, and the mixture was stirred at room temperature for 30 min. The resulting fluid gel was charged into 30-mL Teflon-lined autoclaves and heated at 175 °C for 7 days under agitation. The obtained solid product was recovered by filtration, washed with distilled water, and dried overnight (90 °C). To remove the SDA, the as-synthesized zeolite was calcined in a stream of air at 550 °C for 6 h with a temperature ramp of 1 °C/min.

**Synthesis of IPC-1P Precursor.** IPC-1P precursor was prepared as described elsewhere.[43] Calcined **UTL** was hydrolyzed in 0.1 M HCl with the w/w ratio around 1/200 at 90 °C overnight. The product was isolated by centrifugation, washed out with distilled water, and dried at 60 °C.

**Swelling of IPC-1P Precursor.** The swollen material, ICP-1SW, was prepared by treating IPC-1P with a mixture of 40 wt % tetrapropylammonium hydroxide (TPA−OH) and 25 wt % hexadecyltrimethylammonium chloride (CTMA-Cl) (w/w = 1/9) in the ratio 1/50 (w/w). The mixture was stirred at ambient temperature overnight (10 h). The product was isolated by centrifugation, washed with water, and dried at 80 °C.

**Synthesis of Pillared Materials Using BSSs and POS.** ICP-1SW (0.2 g) was vigorously stirred with a chloroform solution (5 mL) of 0.2−0.4 g of 1,4-bis-(triethoxysilyl)benzene (BSS1), 1,2-bis-(triethoxysilyl)ethane (BSS2), 4,4-bis-(triethoxysilyl)-1,1'-biphenyl (BSS3) or octakis(tetramethylammonium)T8-siloxane (POS) for 2 days at 60 °C. Solvent was partially evaporated at 40 °C and 20 Torr. The white solid obtained was dried for 2 days at 65 °C.

**Removal of the Swelling Agent.** To remove CTMA, the pillared material (0.2 g) was suspended in 30 mL of 1 M $NH_4NO_3$ solution in ethanol/$H_2O$ (w/w = 1/1) for 2 days at room temperature (ammonia salt was used for ionic exchange with CTMA cations, ethanol was used for the shift of respective equilibrium due to the increasing of CTMA solubility). The solid, separated by centrifugation, was treated with 0.2
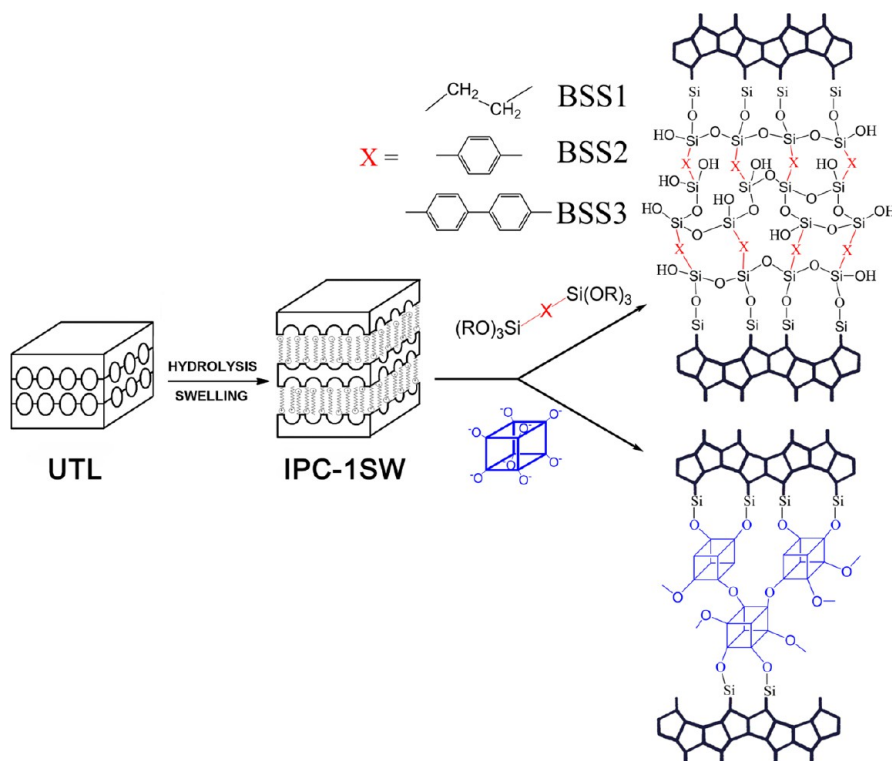
**Figure 1.** Representation of methodology to obtain hybrid organic–inorganic (organic linkers, top arrow) or pillared inorganic (using polyhedral oligomeric siloxane, bottom arrow) material obtained from IPC-1P precursor.

M HCl solution in ethanol/octane mixture (w/w = 1/1) for 2 days at 60 °C (the purpose of this step was similar to the previous one but with the different nature of eluent). The final product was filtered off, washed with water, ethanol/octane (w/w = 1/1) solution, ethanol and then dried at 65 °C overnight.

The materials obtained are denominated XUTL-HY, where X = w/w ratio for intercalating agent/IPC-1SW (1, 1.5, 2) and Y = 1 for BSS1, 2 for BSS2, 3 for BSS3 and 4 for POS.

**Characterization.** X-ray powder diffraction data were collected on a Bruker AXS D8 Advance diffractometer with a Vantec-1 detector in the Bragg–Brentano geometry using Cu Kα ($\lambda$ = 0.154178 nm) radiation. Adsorption isotherms of nitrogen at −196 °C (argon at −196/−186 °C) were recorded using an ASAP 2020 (Micromeritics) static volumetric apparatus. Before adsorption, the samples were degassed with a turbomolecular pump at 150−350 °C for 8 h. Micropore size distribution was evaluated using the NLDFT method (Carb Cylinder Pores MWNT kernel). To calculate the adsorption isosteres, Ar sorption isotherms (at −196/−186 °C) were transformed to $\log(p) = a$ coordinates, where $a$ = adsorbed amounts; $a$ = 5, 10, 15,..., 55 cm$^3$/g STP. The values of $\log(p)$ were calculated using a polynomial interpolation procedure. The isosteric heats of adsorption ($Q_{st}$) were calculated from the slope of the adsorption isosteres using the equation

$$\frac{d(\log p)}{d(1/T)} = -\frac{(Q_{st})}{2.303 \cdot R}$$

where ($R$ = gas constant).

Morphological characterization was carried out by scanning electron microscopy (SEM), using a field emission scanning electron microscope JEOL 7600F. The samples were prepared by dispersing the powder in ethanol and evaporating the suspension on the specimen holder. The images were collected with an acceleration voltage of 5 kV. Transmission electron microscopy (TEM) was performed with a TEM Zeiss Libra 120. Powder samples were embedded in epoxy resin, and 40 nm thick sections were obtained with a Reichert-Jung ULTRACUT ultramicrotomer equipped with a diamond knife.

$^{13}$C MAS NMR spectra were collected using an Agilent V-500 (at 126 MHz, 3.7 μs 90° pulse with a DEPTH filter,[46] 30 s delay, spinal $^1$H decoupling and shifts referenced to tetramethylsilane (0 ppm) using adamantane (at 38.5 and 29.4 ppm) for powders contained in 4 mm rotors spinning at 14 kHz. A Bruker ASX-300 was used to observe $^{29}$Si (59 MHz, 3.8 μs 60° pulse, 90 s delay, mlev16 $^1$H decoupling, shifts referenced to tetramethylsilane at 0 ppm using tetrakis-(trimethylsilyl)silane at −9.8 and −135.2 ppm) for samples contained in 7 mm rotors spinning at 5 kHz.

Thermogravimetric analyses were performed on a TG-750 Stanton Redcroft thermobalance in air between 20 and 900 °C with a heating rate of 10 °C/min. The weight of the sample was about 5 mg.
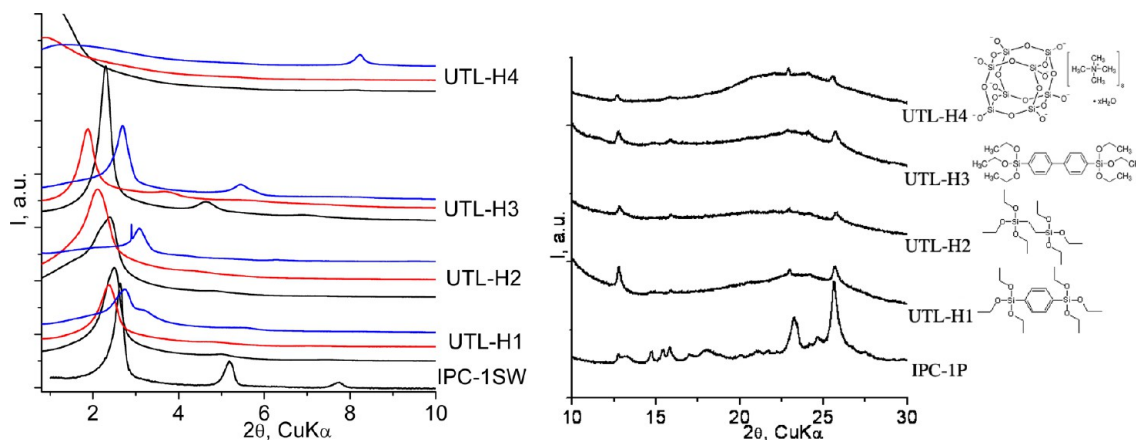
## ■ RESULTS AND DISCUSSION

**Synthesis of Swollen IPC-1P Zeolitic Precursor and Intercalation with BSSs/POS.** The synthesis of pillared materials, by intercalating the IPC-1P layered precursor with
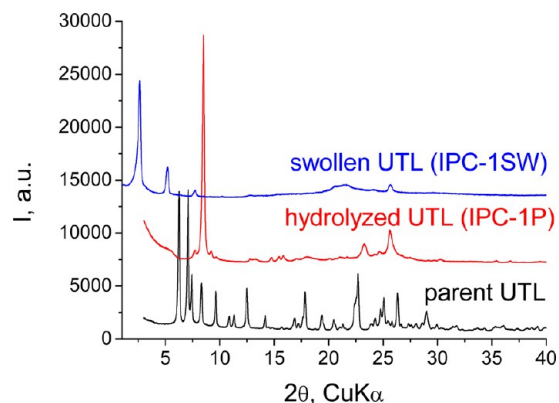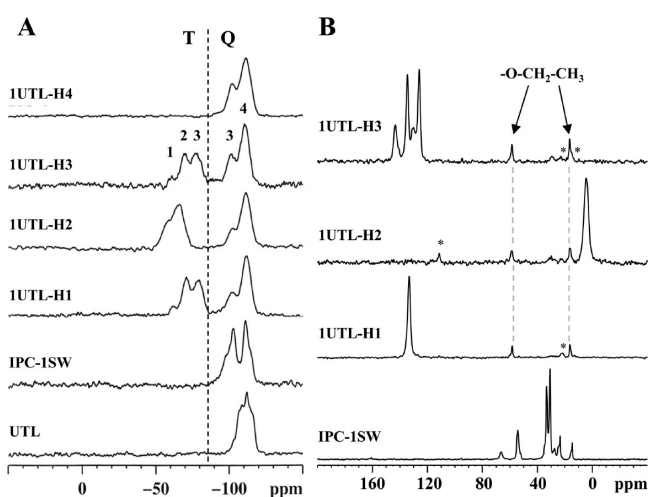


**Figure 2.** XRD patterns of the UTL, IPC-1P, and IPC-1SW.

**Figure 3.** XRD patterns (low angle region: left; medium angle region: right) of the IPC-1P, IPC-1SW (intensities reduced for clarity) and synthesized hybrid materials with different intercalating agent/IPC-1SW w/w ratio: 1: black; 1.5: red; 2: blue.



**Figure 4.** Solid-state $^{29}$Si (A) and $^{13}$C (B) MAS NMR spectra of parent and materials derived from UTL. CSiO$_3$ sites are labeled T and SiO$_4$ sites are Q with the number of Si−O−Si connections per site indicated. Asterisks denote spinning side bands.

BSS or POS, was performed after hydrolyzing and swelling the **UTL** zeolite (Figure 1). The **UTL** structure can be described as continuous 2D layers connected by cubic double-four-ring units
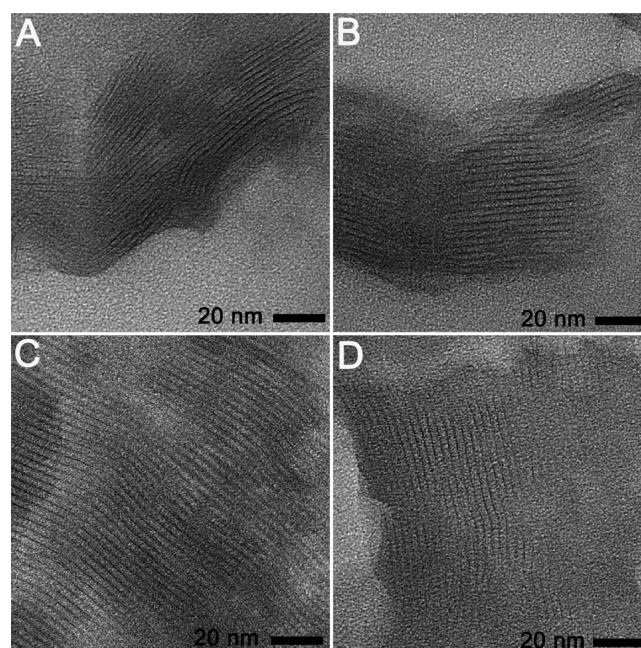


**Figure 6.** TEM images of IPC-1SW (A), 1UTL-H1 (B), 1UTL-H2 (C), and 1UTL-H3 (D).
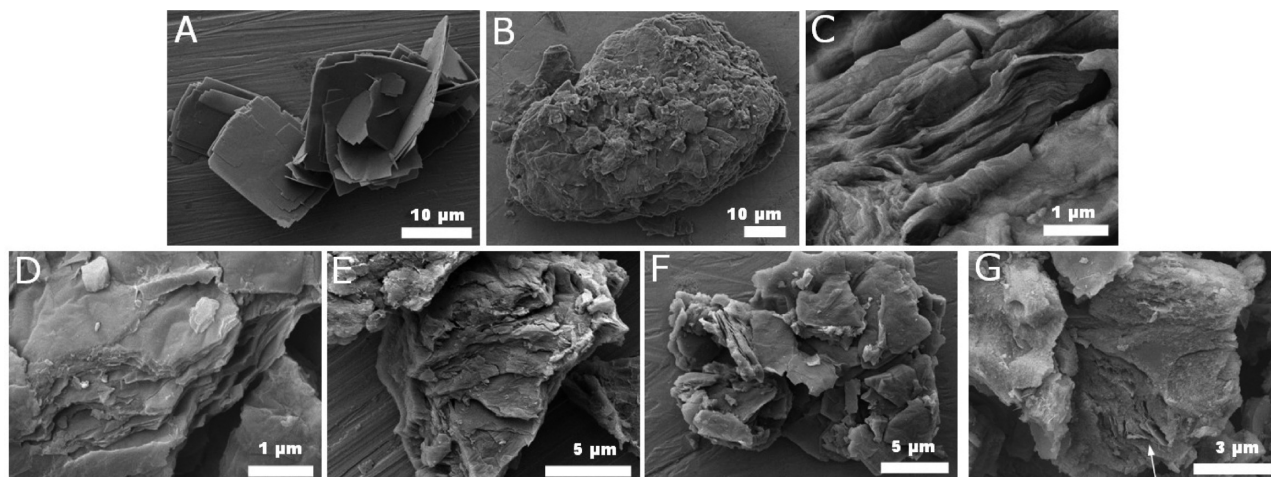


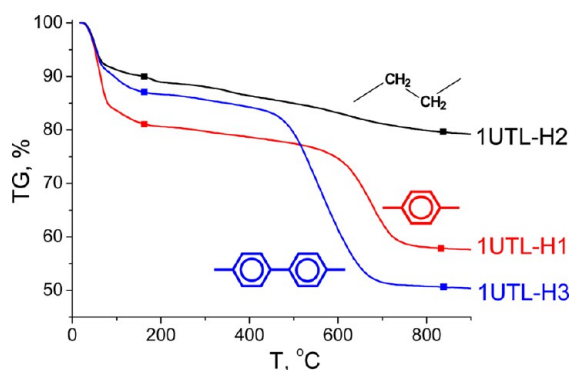**Figure 5.** SEM images of UTL zeolite (A), IPC-1SW (B, C), 1UTL-H1 (D), 1UTL-H2 (E), 1UTL-H3 (F), 1UTL-H4 (G).

**Figure 7.** Thermogravimetric curves for the 1UTL hybrid materials.

**Table 1. Textural Properties of UTL, IPC-1SW and Intercalated Hybrids (calculated from N$_2$ sorption isotherms at −196 °C)**

| material | $S_{BET}{}^a$, m$^2$/g | $V_{total}{}^b$, cm$^3$/g | $V_{micro}{}^c$, cm$^3$/g |
|---|---|---|---|
| UTL | 458 | 0.202 | 0.193 |
| IPC-1SW | 216 | 0.130 | 0.007 |
| 1UTL-H1 | 645 | 0.430 | 0.229 |
| 1.5UTL-H1 | 1077 | 0.668 | 0.053 |
| 2UTL-H1 | 700 | 0.503 | 0.207 |
| 1UTL-H2 | 765 | 0.644 | 0 |
| 1.5UTL-H2 | 851 | 0.748 | 0 |
| 2UTL-H2 | 520 | 0.518 | 0.149 |
| 1UTL-H3 | 747 | 0.464 | 0.303 |
| 1.5UTL-H3 | 869 | 0.584 | 0.319 |
| 2UTL-H3 | 693 | 0.526 | 0.212 |
| 1UTL-H4 | 456 | 1.018 | 0.018 |
| 1.5UTL-H4 | 376 | 0.867 | 0.015 |
| 2UTL-H4 | 395 | 0.697 | 0.023 |

$^a$Surface area was evaluated using adsorption branch in the range $p/p_s$ = 0.05−0.35. $^b$Total pore volume vas evaluated at $p/p_s$ = 0.95. $^c$Micropore volume was evaluated from the t-plot method.
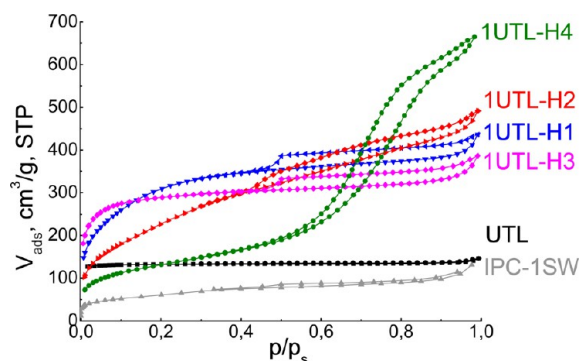


**Figure 8.** N$_2$ sorption isotherms (−196 °C) for UTL, calcined IPC-1SW and intercalated hybrids.

(D4R). Ge atoms in the **UTL** framework are preferentially located in D4Rs[47−49] and are also the sites with the lowest stability.[25,43] Since the Ge−O bond is less hydrolytically stable than the Si−O bond, D4Rs can be selectively removed while preserving mainly the layers containing Si atoms.[25]

The successful transformation of **UTL** to IPC-1P was confirmed using XRD (Figure 2). The diffraction pattern of parent **UTL** has the (200) reflection at 6.2° 2$\theta$ (spacing between centers of the layers is 1.42 nm). After hydrolysis, the XRD pattern of the IPC-1P changes considerably. The

diffraction pattern of IPC-1P contains a strong diffraction line located at 2$\theta$ = 8.3°, spacing between the centers of layers is 1.06 nm) together with a number of weak reflections (intralayer reflections). The significant shift in maxima attributed to the interlayer (100) plane corresponds to a 0.36 nm contraction for the **UTL** to IPC-1P transformation.[25]

The hydrolyzed material (IPC-1P), consisting of ultrathin zeolite layers, was then treated with cetyltrimethylammonium (CTMA) chloride/hydroxide to yield the swollen material IPC-1SW.[25] The corresponding XRD pattern (Figure 2) contains dominant reflections considerably shifted to a lower angle, indicating a significant expansion of the interlayer distance caused by intercalation of the cationic surfactant.

Intercalation of IPC-1SW with BSSs or POS, subsequent hydrolysis and removal of the CTMA swelling agent (by consecutive extraction using NH$_4$NO$_3$ and HCl solutions) provided self-organized mesophasic materials with a zeolitic intralayer structure (Figure 3). The positions of low-angle diffraction lines for the swollen samples correspond to interlayer distances (d-spacings are equal to 3.47 and 3.52−3.77 nm for IPC-1SW and 1UTL-H1−3, respectively) which do not match the sizes of single silsesquioxane molecules. We assume that the intercalating agent fills the available interlayer space instead of forming layer−agent−layer clusters with only one silsesquioxane molecule between sheets. The "pillars" are covalently bonded to the layer surface by condensation of terminal alkoxide/silicate groups (from silsesquioxanes) with the Si−OH groups of IPC-1P. Since the thickness of UTL layers is about 1 nm, the interlayer distance is about 2.5 nm for IPC-1SW and 1UTL-H1, 2.8 nm for 1UTL-H2, and 2.6 nm for 1UTL-H3. This means the number of the silsesquioxane molecules connecting the two layers is approximately 3, 4, and 2 for linkers containing phenylene (the distance between two opposing oxygen atoms in BSS1 molecule is ∼0.82 nm), ethanediyl (0.65 nm) and (1.26 nm) fragments, respectively.

The corresponding positions of diffraction lines for IPC-1P and synthesized materials (Figure 3) confirms the preservation of zeolitic layers in the hybrids obtained. Positions of low-angle diffraction lines for UTL-H1−3 materials were affected by intercalating agent/IPC-1SW ratio and differed from that for parent IPC-1SW. The increasing of d-spacing (the left-shift of respective low-angle diffraction line) with enhancement of intercalating agent/IPC-1SW ratio from 1 to 1.5 and subsequent lowering of interplanar distance with further increasing of intercalating agent/IPC-1SW ratio to 2 was a general trend for all used intercalants. It seems that an increasing in the relative stability of the formed pillars is observed with increasing the amount of BSS molecules between layers (larger d-spacing for materials obtained using intercalating agent/IPC-1SW ratio 1.5 respect to 1). Further increase in BSS molecules content probably leads to a change in their reciprocal arrangement and a consequent minor swelling expansion for materials obtained using intercalating agent/IPC-1SW ratio 2.

Intensities of low-angle diffraction lines depend on the amount of BSS molecules, and in most cases they decrease with increasing content of the intercalating agent (Figure 3). Similarly to what is observed in hybrid materials, even the samples UTL-H4 present the intralayer IPC-1P reflections in the high angle region of the XRD pattern (Figure 3) demonstrating that the **UTL** layers are preserved after swelling and pillaring with POS. On the contrary, the low angle region of the same XRD patterns is of difficult interpretation.
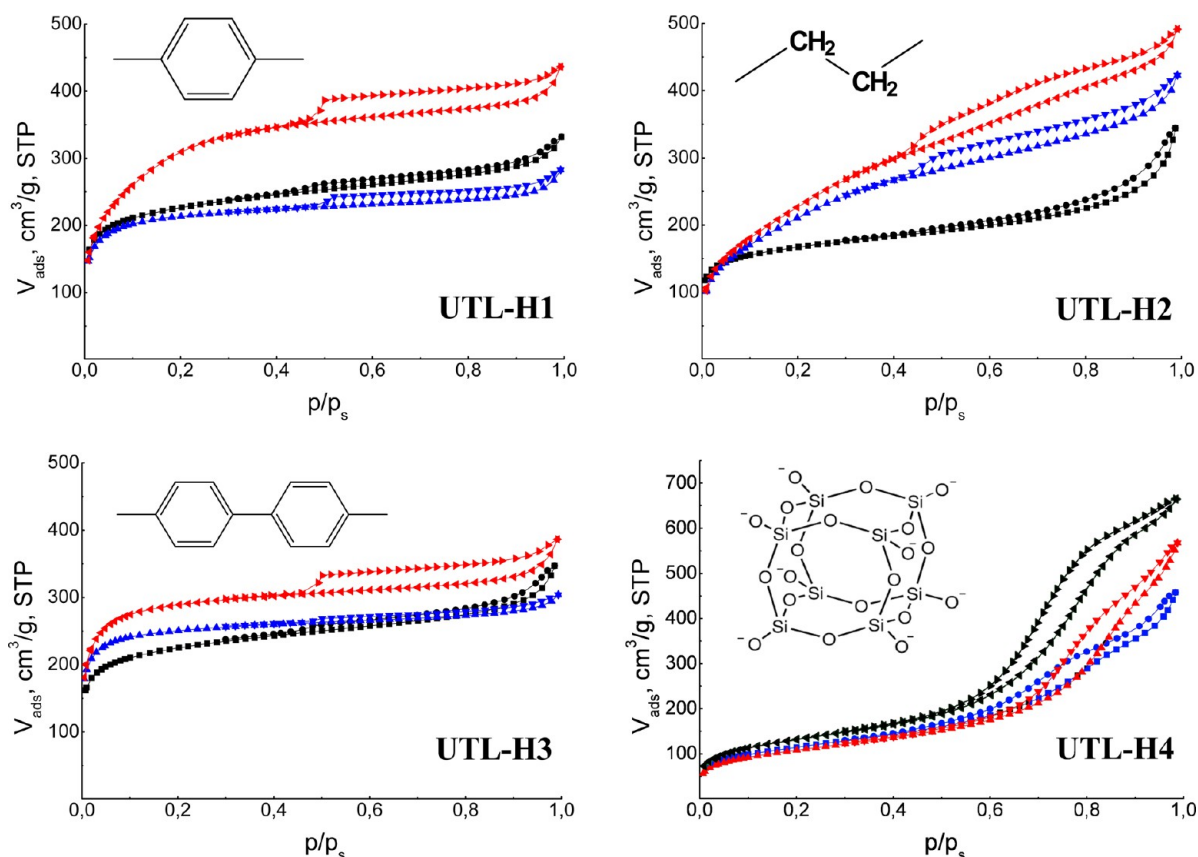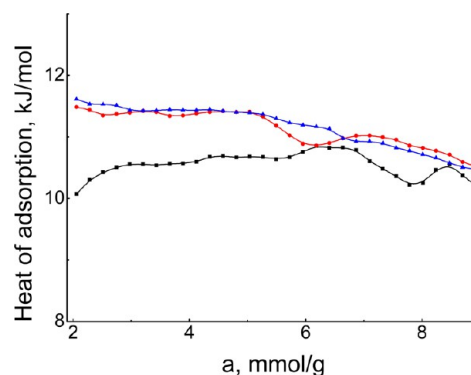
**Figure 9.** N$_2$ sorption isotherms (−196 °C) for the four hybrids obtained with different amounts of intercalating agent (X = 1 black, 1.5 red, 2 blue).
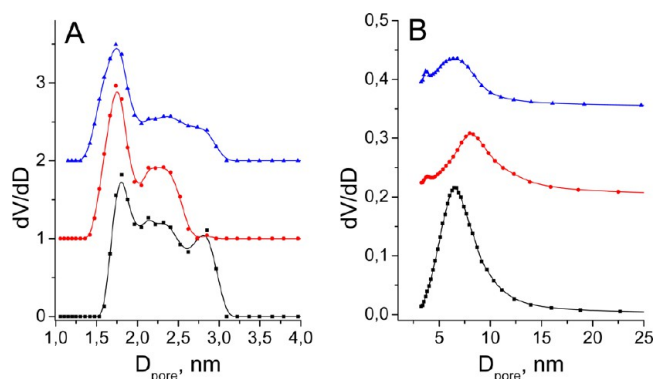


**Figure 10.** Pore size distribution with increased amount of intercalation agent (X = 1 black, 1.5 red, 2 blue) for UTL-H3 (A) and UTL-H4 (B) obtained from Ar sorption isotherms at −186 °C.

**Figure 11.** Isosteric heats of adsorption (Ar) versus coverage for UTL-H3 materials obtained with different amounts of linkers (intercalating agent/IPC-1SW w/w ratio: black −1, red −1.5, blue −2).

Although there are scattering phenomena in this region (Figure 3), their weak and diffuse nature makes it impossible to draw an accurate structural model for UTL-H4 materials. Starting from the evidence derived from the XRD analysis, it is likely that they are constituted by a disordered stacking of **UTL** layers with variable interlayer spacing and relative orientation.

The pillaring of **UTL** layers in the materials (with X = 1) was confirmed by solid-state MAS NMR spectroscopy (Figure 4). Si atoms attached to four O atoms are designated Q while Si atoms attached to three O atoms and one carbon are designated T. A superscript indicates the number of framework (Si−O−Si) connections. Thus, a Q$^3$ site is Si(OSi)$_3$OH and a T$^2$ site is CSi(OSi)$_2$(OH). The swollen UTL (IPC-1SW) had only 50% Q$^4$ Si (Figure 4A, Table S1 in SI), instead of the 75%

Q$^4$ Si estimated if the acid dislodged only the germanate D4R units during the hydrolysis. The large amount of Q$^3$ sites observed for IPC-1SW may be explained in two ways. First, Ge atoms (which are relatively easy to extract from the framework during hydrolysis[26]) are present not only in the double four rings but also to some extent in the layers leading to additional Q$^3$ formation. Second, the conditions used for hydrolysis and swelling (acidic and basic, respectively) along with the mechanical lability of the thin layers derived from IPC-1P can produce large amount of defects.

As expected, the amounts of Q$^3$ and Q$^2$ sites in IPC-1SW largely decreased after pillaring. This confirms the condensation of the bis-silylated organic precursors or POS with the silanol groups on the zeolite layer surface. In addition, the $^{29}$Si shifts
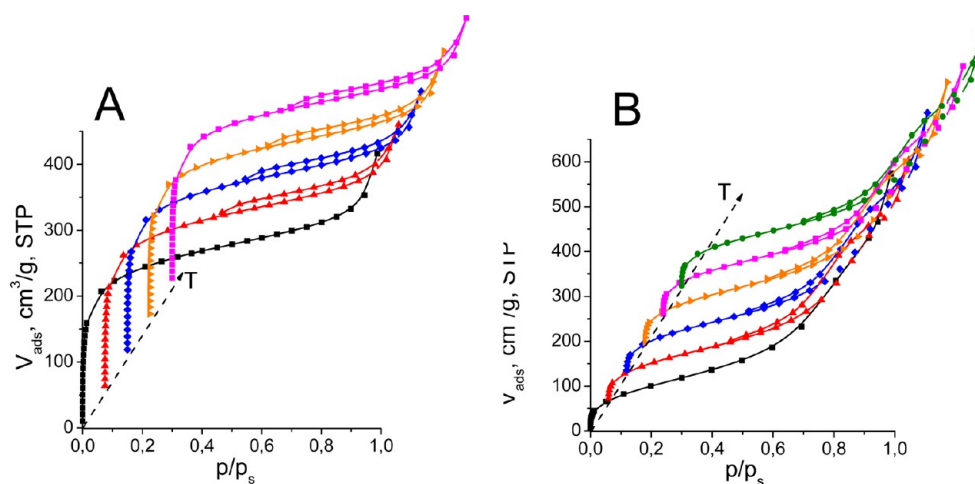
**Figure 12.** Ar sorption isotherms (−186 °C) for 2UTL-H3 (A) and 2UTL-H4 (B) samples activated at 100 (black), 150 (red), 200 (blue), 250 (orange), 300 (magenta), 350 °C (green).

(Table S1 in SI) of the $T^3$ sites for phenylene H1 (−80 ppm), ethylene H2 (−66 ppm) and biphenylene H3 (−78 ppm) hybrids (H1−H3) agree with those in the literature.[50,23,51] Complete spectral deconvolution (e.g., UTL-H1, Figure S1 in SI) gave the shifts and spectral areas for all peaks (Table S1 in SI).

^{13}C NMR spectra (Figure 4B) reveal that the organic−inorganic hybrids contain up to 10% mol of uncondensed Si−OCH$_2$CH$_3$ groups (signals at 59 and 16 ppm) due to incomplete precursor hydrolysis. It is quite reasonable that some Si−OR groups remain since their hydrolysis and condensation inside the interlayer space can be limited by steric hindrance.

Chemical shifts of corresponding C-atoms in the organic linkers (ethylene, 5 ppm; phenylene, 133 ppm; and biphenylene, 143, 134, 126, 130 ppm) match well with literature data for ethylene,[50] phenylene,[23] and biphenylene.[51] Only trace amounts of CTMA were detected in the hybrids by ^{13}C NMR (small peaks at 32 ppm), confirming nearly complete removal of the swelling agent from the interlayer space (Figure 4B).

Crystal shapes of **UTL**, IPC-1SW, and pillared materials were compared by SEM. Figure 5A,B shows that parent **UTL** zeolite crystallizes as platelet-like crystals, whereas IPC-1SW was much less regular in crystal shape. Nevertheless, in the swollen sample, the well-resolved layered morphology can still be observed (Figure 5C).

The crystals of hybrids obtained by intercalation with the BSSs possessed layered morphology similar to that of IPC-1SW (Figure 5D−F) in contrast to 1UTL-H4 which exhibited no layered morphology and rare small inclusions (marked by arrow in Figure 5G). The presence of a small amount of nonintercalated species cannot be excluded in the UTL-H4 sample.

TEM images (Figure 6) indicated that IPC-1SW and the BSS hybrids (UTL-H1−3) have similar *d*-spacings of about 3 nm, which do not correspond exactly with the distances evaluated from XRD patterns (3.5 − 3.8 nm). That is probably due to a partial collapse of the organic clusters pillaring the inorganic **UTL** layers, under the electron beam. The intercalated hybrids contained quite large crystalline domains (Figure 6B−D), in agreement with the preservation of IPC-1SW's crystal morphology after intercalation with BSS and CTMA removal.

1UTL-H4 exhibited highly defective periodicity being mainly amorphous.

The amount of bridged silsesquioxane molecules located between layers was estimated using thermogravimetric analysis (Figure 7). Assuming that weight loss below 150 °C may be attributed to water removal, the weight loss due to organic linker destruction was about 11% for hybrid material with ethylene bridges, 23% for phenylene, and 36% for biphenylene-containing samples. This corresponds to 4, 3, and 2.5 mmol/g for 1UTL-H2, H1, and H3, respectively. These values decreased predictably with increasing linker size and are consistent with the quantity of BSS molecules between layers (∼4, 3, and 2 for 1UTL-H2, H1, and H3, respectively) calculated from XRD patterns.

The zeolitic hybrids under investigation are porous materials with widely varying textural properties (Table 1). Typical adsorption−desorption isotherms are presented in Figure 8.

Residual porosity of the sample IPC-1SW after calcination may be explained by the interparticle adsorption of the respective collapsed and partially delaminated material. The intercalating agent/IPC-1SW ratio (X) significantly influenced the textural properties of the hybrids (Table 1), but not the isotherm type (Figure 9). While UTL-H1 and UTL-H3 materials showed isotherms of type I with hysteresis loop of H4, which is typical for materials possessing micropores with broad size distribution. UTL-H2 samples were characterized by nonreversible isotherms of type II with H3 hysteresis loop indicating the broad mesopore size dictribution. UTL-H4 samples were characterized by isotherms of type IV with quite narrow mesopore size distribution. Initial rise of isotherm for 1.5UTL-H1 sample having lower micropore volume in comparison with 1UTL-H1 and 2UTL-H1 materials was similar to mentioned samples that can be explained by the larger surface area (1077 m$^2$/g) of 1.5UTL-H1 in comparison with 1UTL-H1 (645 m$^2$/g) and 2UTL-H1 (700 m$^2$/g). The highest surface area and pore volume for a BSS hybrid (UTL-H1−3) was obtained with X = 1.5. This might be explained by an optimum combination of stability and porosity, since a lower content of bridged molecules can decrease rigidity and stability of the hybrid material. A higher loading of BSS molecules may lead to an increased amount of pillars or to the formation of a nonporous phase. In the case of POS-containing materials, the highest porosity was obtained with the lowest content of

intercalation agent, probably because the pillars formed were more rigid than for the silsesquioxane-based hybrids. In most cases, an increase in the content of BSSs/POS resulted in the formation of additional micropores that are most probably defined by the pillars. $S_{BET}$ and $V_{total}$ were comparable for the hybrids (Table 1) and significantly exceeded those for the parent zeolite and IPC-1SW (after calcination). The amount of micropores increased with increasing rigidity and size of the organic linker in the order: biphenyl > phenylene > ethanediyl (Table 1). The POS-containing compound was a typical mesoporous material (Figure 9) with a relatively narrow pore size distribution.

The textural characteristics of the hybrids can be compared with those for recently reported materials with similar structures.[30,43] **MWW**-based organic−inorganic hybrids exhibited: $S_{BET}$ up to 550 m$^2$/g, $V_{micro}$ and $V_{total}$ up to 0.070 and 0.321 cm$^3$/g, respectively.[30] Inorganic pillared IPC-1P-based materials displayed: $S_{BET} \approx$ 1100 m$^2$/g, $V_{micro}$ up to 0.014 cm$^3$/g and $V_{total}$ up to 0.85 cm$^3$/g.[43] Our IPC-1P-based materials reached: $S_{BET}$ up to 1080 m$^2$/g, $V_{micro}$ up to 0.319 cm$^3$/g and $V_{total}$ up to 1.018 cm$^3$/g (Table 1) making them promising candidates for application in sorption and catalysis (after functionalization). In addition, we evidenced that the volume of both micro and mesopores can be tuned by the synthesis protocol.

The pore size distribution of the BSS hybrid was not sharp. It should be noted that the relative content of large diameter pores decreased with increasing amount/thickness of pillars (Figure 10A). 1UTL-H4 is a classic mesoporous solid with 5−10 nm pores. The higher rigidity of POS pillars, compared with BSS pillars, invoked above could also explain the narrow pore size distribution found for the sample with the smallest amount of POS intercalation molecules (Figure 10).

Heats of Ar adsorption calculated for UTL-H3 with different content of BSS (Figure 11), increased slightly with increasing intercalating agent/IPC-1SW ratio (X). Adsorption heat remains almost unchanged with coverage, at high BSS loading the energetic homogeneity of the surface slightly increased.

The thermal stability of the pore systems for selected hybrids was examined. For this purpose sorption isotherms of 2UTL-H3 (Figure 12A) and 2UTL-H4 (Figure 12B), activated at different temperatures (100−350 °C with the 50+ °C step) were collected. As it can be seen (Figure 12) neither the shape of isotherms, nor absolute values of adsorption were significantly affected by activation temperatures under the conditions used (the ad/desorption curves on Figure 12 are displayed with an offset for clarity), evidencing the stability of the pore system of 2UTL-H3 and 2UTL-H4 up to 350 °C.

## CONCLUSIONS

Novel porous pillared materials containing organic linkers or polyhedral oligomeric siloxane covalently bonded to zeolitic layers of IPC-1P were obtained from **UTL** layers (IPC-1P) prepared by a top-down procedure. Obtained materials exhibited a mesoporous or hierarchical micro-/mesoporous system with excellent textural characteristics ($S_{BET}$ > 1000 m$^2$/g, $V_{micro}$ > 0.3 cm$^3$/g, $V_{total}$ > 1 cm$^3$/g). Despite the obvious potential of such materials, some challenges still need to be overcome. First of all, functionalization will allow us to obtain catalytically active materials with easily tunable porosities. Second, the further investigation for control of pore size (modulated by different precursors and SDA's, and their

relative amounts) could open the way to new shape-selective materials for sorption/catalytic applications.

## ASSOCIATED CONTENT

### Supporting Information

$^{29}$Si MAS NMR data obtained from deconvolution of the spectra shown in Figure 4A are provided in Table S1. $^{29}$Si MAS NMR spectrum of 1UTL-H1 from Figure 4A with spectral deconvolution and signal assignments are given in Figure S1. Figure S2 shows $^1$H NMR spectrum of 7-ethyl-6-azoniaspiro-[5.5]-undecane hydroxide used as SDA for the synthesis of UTL zeolite. This material is available free of charge via the Internet at http://pubs.acs.org.

## AUTHOR INFORMATION

### Corresponding Author

jiri.cejka@jh-inst.cas.cz

### Notes

The authors declare no competing financial interest.

## ACKNOWLEDGMENTS

## REFERENCES

(1) Bellussi, G.; Carati, A.; Rizzo, C.; Millini, R. *Catal. Sci. Technol.* **2013**, *3*, 833.
(2) Sanchez, C. C.; Julian, B.; Belleville, P.; Popall, M. *J. Mater. Chem.* **2005**, *15*, 3559.
(3) Margelefsky, E. L.; Zeidan, R. K.; Davis, M. E. *Chem. Soc. Rev.* **2008**, *37*, 1118.
(4) Boronat, M.; Climent, M. J.; Corma, A.; Iborra, S.; Monton, R.; Sabater, M. J. *Chem.—Eur. J.* **2010**, *16*, 1221.
(5) Climent, M. J.; Corma, A.; Iborra, S.; Mifsud, M. *J. Catal.* **2007**, *247*, 223.
(6) Čejka, J.; Centi, G.; Perez-Pariente, J.; Roth, W. *J. Catal. Today* **2012**, *179*, 2.
(7) Eddaoudi, M.; Moler, D. B.; Li, H.; Chen, B.; Reineke, T. M.; O'Keeffe, M.; Yaghi, O. M. *Acc. Chem. Res.* **2001**, *34*, 319.
(8) Hoffmann, F.; Cornelius, M.; Morell, J.; Fröba, M. *Angew. Chem., Int. Ed.* **2006**, *45*, 3216.
(9) Corma, A.; Iglesias, M.; del Pino, C.; Sanchez, F. *J. Chem. Soc., Chem. Commun.* **1991**, 1253.
(10) Sanchez, F.; Iglesias, M.; Corma, A.; del Pino, C. *J. Mol. Catal.* **1991**, *70*, 369.
(11) Carmona, A.; Corma, A.; Iglesias, M.; San Jose, A.; Sanchez, F. *J. Organomet. Chem.* **1995**, *492*, 11.
(12) Cauvel, A.; Brunel, D.; Di Renzo, F.; Moreau, P.; Fajula, F. *Stud. Surf. Sci. Catal.* **1994**, *94*, 286.
(13) Jones, C. W.; K. Tsuji, K.; Davis, M. E. *Nature* **1998**, *393*, 52.
(14) Jones, C. W.; K. Tsuji, K.; Davis, M. E. *Microporous Mesoporous Mater.* **1999**, *29*, 339.
(15) Jones, C. W.; K. Tsuji, K.; Davis, M. E. *Microporous Mesoporous Mater.* **1999**, *33*, 223.
(16) Jones, C. W.; K. Tsuji, K.; Davis, M. E. *Microporous Mesoporous Mater.* **2001**, *42*, 21.
(17) Yamamoto, K.; Sakata, Y.; Nohara, Y.; Takahashi, Y.; Tatsumi, T. *Science* **2003**, *300*, 470.
(18) Yamamoto, K.; Nohara, Y.; Domon, Y.; Takahashi, Y.; Sakata, Y.; Plévert, J.; Tatsumi, T. *Chem. Mater.* **2005**, *17*, 3913.
(19) Yamamoto, K.; Tatsumi, T. *Chem. Mater.* **2008**, *20*, 972.
(20) Díaz, U.; Vidal-Moya, J. A.; Corma, A. *Microporous Mesoporous Mater.* **2006**, *93*, 180.
(21) Su, B. L.; Roussel, M.; Vause, K.; Yang, X. Y.; Gilles, F.; Shi, L.; Leonova, E.; Edén, M.; Zou, X. *Microporous Mesoporous Mater.* **2007**, *105*, 49.

(22) Bellussi, G.; Carati, A.; Di Paola, E.; Millini, R.; Parker, W. O., Jr.; Rizzo, C.; Zanardi, S. *Microporous Mesoporous Mater.* **2008**, *113*, 252.

(23) Bellussi, G.; Montanari, E.; Di Paola, E.; Millini, R.; Carati, A.; Rizzo, C.; Parker, W. O., Jr.; Gemmi, M.; Mugnaioli, E.; Kolb, U.; Zanardi, S. *Angew. Chem., Int. Ed.* **2012**, *51*, 666.

(24) Bellussi, G.; Millini, R.; Montanari, E.; Carati, A.; Rizzo, C.; Parker, W. O., Jr.; Cruciani, G.; de Angelis, A.; Bonoldi, L.; Zanardi, S. *Chem. Commun.* **2012**, *48*, 7356.

(25) Roth, W. J.; Shvets, O. V.; Shamzhy, M.; Chlubná, P.; Kubů, M.; Nachtigall, P.; Čejka, J. *J. Am. Chem. Soc.* **2011**, *133*, 6130.

(26) Roth, W. J.; Nachtigall, P.; Morris, R. E.; Wheatley, P. S.; Seymour, V. R.; Ashbrook, S. E.; Chlubná, P.; Grajciar, L.; Položij, M.; Zukal, A.; Shvets, O.; Čejka, J. *Nat. Chem.* **2013**, *5*, 628.

(27) Ramos, F. S. O.; de Pietre, M. K.; Pastore, H. O. *RSC Adv.* **2013**, *3*, 2084.

(28) Ruiz-Hitzky, E.; Darder, M.; Aranda, P. *J. Mater. Chem.* **2005**, *15*, 3650.

(29) Díaz, U.; Cantín, A.; Corma, A. *Chem. Mater.* **2007**, *19*, 3686.

(30) Corma, A.; Díaz, U.; García, T.; Sastre, G.; Velty, A. *J. Am. Chem. Soc.* **2010**, *132*, 15011.

(31) He, H.; Ding, Z.; Zhu, J.; Yuan, P.; Xi, Y.; Yang, D.; Frost, R. L. *Clays Clay Miner.* **2005**, *53* (2005), 287.

(32) Srivastava, V.; Gaubert, K.; Pucheault, M.; Vaultier, M. *ChemCatChem* **2009**, *1*, 94.

(33) Naranjo, P. M.; Sham, E. L.; Castellón, E. R.; Torres Sánchez, R. M.; Farfán Torres, E. M. *Clays Clay Miner.* **2013**, *61*, 98.

(34) Ogawa, M.; Kuroda, K. *Bull. Chem. Soc. Jpn.* **1997**, *70*, 2593.

(35) Jianxi, Z.; Yanhong, Q.; Tong, W.; Runliang, Z.; Jingming, W.; Qi, T.; Peng, Y.; Hongping, H. *J. Colloid Interface Sci.* **2011**, *360*, 386.

(36) Kłapyta, Z.; Gaweł, A.; Fujita, T.; Iyi, N. *Clay Miner.* **2003**, *38*, 151.

(37) Li, L.; Ma, R.; Ebina, Y.; Iyi, N.; Sasaki, T. *Chem. Mater.* **2005**, *17*, 4386.

(38) Ruiz-Hitzky, E.; Rojo, J. M. *Nature* **1980**, *287*, 28.

(39) Shimojima, A.; Mochizuki, D.; Kuroda, K. *Chem. Mater.* **2001**, *13*, 3603.

(40) Ishii, R.; Shinohara, Y. *J. Mater. Chem.* **2005**, *15*, 551.

(41) Ishii, R.; Ikeda, T.; Itoh, T.; Ebina, T.; Yokoyama, T.; Hanaoka, T.; Mizukami, F. *J. Mater. Chem.* **2006**, *16*, 4035.

(42) Mochizuki, D.; Kowata, S.; Kuroda, K. *Chem. Mater.* **2006**, *18*, 5223.

(43) Chlubná, P.; Roth, W. J.; Greer, H. F.; Zhou, W.; Shvets, O.; Zukal, A.; Čejka, J.; Morris, R. E. *Chem. Mater.* **2013**, *25*, 542.

(44) Shamzhy, M. V.; Shvets, O. V.; Opanasenko, M. V.; Yaremov, P. S.; Sarkisyan, L. G.; Chlubná, P.; Zukal, A.; Hartmann, M.; Čejka, J. *J. Mater. Chem.* **2012**, *22*, 15793.

(45) Shvets, O. V.; Kasian, N.; Zukal, A.; Pinkas, J.; Čejka, J. *Chem. Mater.* **2010**, *22*, 3482.

(46) The DEPTH filter is a composite (90°−180°−180°) excitation pulse with 16-step phase cycling (onepuldpth Agilent pulse program) to suppress the background signal from the Kel-F spacers, adapted from Cory, D. G.; Ritchey, W. M. *J. Magn. Reson.* **1988**, *80*, 128.

(47) Blasco, T.; Corma, A.; Díaz-Cabanas, M. J.; Rey, F.; Vidal-Moya, J. A.; Zicovich-Wilson, C. M. *J. Phys. Chem. B* **2002**, *106*, 2634.

(48) O'Keeffe, M.; Yaghi, O. M. *Chem.—Eur. J.* **1999**, *5*, 2796.

(49) Jiang, J.; Yu, J.; Corma, A. *Angew. Chem., Int. Ed.* **2010**, *49*, 3120.

(50) Diaz-Morales, U.; Bellussi, G.; Carati, A.; Millini, R.; Parker, W. O., Jr.; Rizzo, C. *Microporous Mesoporous Mater.* **2006**, *87*, 185.

(51) Okamoto, K.; Goto, Y.; Inagaki, S. *J. Mater. Chem.* **2005**, *15*, 4136.